INTERFACE TRACKING SIMULATIONS OF BUBBLY FLOWS IN THE PWR RELEVANT GEOMETRIES

Jun Fang[1], Michel Rasquin[2], Igor A. Bolotnov[1]
[1]Department of Nuclear Engineering
North Carolina State University
2500 Stinson Drive, Raleigh, NC 27695, USA
jfang3@ncsu.edu; igor_bolotnov@ncsu.edu

[2]Leadership Computing Facility
Argonne National Laboratory
9700 S. Cass Avenue, Argonne, IL 60439, USA
mrasquin@alcf.anl.gov

ABSTRACT

The advances in high performance computing (HPC) have allowed direct numerical simulations (DNS) approach coupled with interface tracking methods (ITM) to perform high fidelity simulations of turbulent bubbly flows in various complex geometries. In this work, we have chosen the geometry of the pressurized water reactor (PWR) core subchannel to perform a set of interface tracking simulations (ITS) with fully resolved turbulence.

The presented research utilizes a massively parallel finite-element based code, PHASTA, for the subchannel geometry simulations of bubbly flow turbulence. The main objective for this research is to demonstrate the ITS capabilities in gaining new insight into bubble/turbulence interactions and assisting the development of improved closure laws for computational multiphase fluid dynamics (CMFD).

Both single- and two-phase turbulent flows were studied within a PWR subchannel. The analysis of numerical results includes the mean gas and liquid velocity profiles, void fraction distribution and turbulent kinetic energy profiles. Two sets of flow rates and bubble sizes were used in the simulations. The chosen flow rates corresponded to the Reynolds numbers of 29,079 and 80,775 based on channel hydraulic diameter and mean velocity. The finite element unstructured grids utilized for these simulations include 53.8 million and 1.11 billion elements, respectively. This has allowed to fully resolving all the turbulence scales and the deformable interfaces of individual bubbles. For the two-phase flow simulations a 1% bubble volume fraction was used which resulted in 17 and 262 bubbles, respectively. In the larger simulation case the size of the resolved bubbles is 0.65 mm in diameter, and the mesh cell size is about 30 microns.

Those large-scale simulations provide new level of details previously unavailable and were enabled by the excellent scaling performance of our two-phase flow solver and access to the state-of-the-art supercomputing resources. The presented simulations used up to 256 thousand processing threads on the IBM BG/Q supercomputer “Mira” (Argonne National Laboratory).

KEYWORDS
DNS, two-phase bubbly flows, subchannel

1. INTRODUCTION

A reliable prediction of the single- and two-phase flows in pressurized water reactor (PWR) rod bundles is critical for both reactor safety and thermal-hydraulics analysis. The turbulent flow in the reactor subchannels has been studied for decades both experimentally and computationally. The distributions of axial velocity, turbulence kinetic energy, and Reynolds stress were measured from the experiments of turbulent flows in subchannels of rod bundles in the past with different aspect ratios (pitch to diameter ratio, P/D) and Reynolds numbers. Trupp and Azad (1975) measured the spatial distributions of mean velocity and Reynolds stresses as functions of Reynolds number and tube spacing for fully developed flow, for which P/D ratios are 1.50, 1.35 and 12, and two Reynolds numbers are used, 12,000 and 84,000 [1]. Carajilescov and Todreas (1976) also did early experiments as well as analytical study to investigate turbulent flows in the subchannel [2]. Detailed experimental data are very important for turbulence modeling and code validation; continued experiments were done by Rehme (1989) [3] and Wu et al. (1993) [4]. The measurement techniques are also being improved over time: Dominguez-Ontiveros and Hassan (2009) have recently done a non-intrusive experimental investigation of flow behavior inside a transparent 5x5 rod bundle with spacer grids using particle image velocimetry (PIV) [5].

Due to the complex and extreme nature of realistic PWR conditions, it is very challenging (if not impossible) and expensive to conduct realistic pressure/temperature conditions experiments to study the turbulent flows in reactor fuel rod bundles. As a result, the computational methodologies are typically chosen as a practical approach to predict flow behavior in PWR conditions. For instance, the advanced thermal-hydraulic subchannel code COBRA-TF [6] is being used worldwide for best-estimation evaluations of nuclear reactor safety margins. Both subchannel and computational fluid dynamics (CFD) methods are being improved as the nuclear industry advances to Generation III+ and Generation IV reactor technology. Avramova recently improved the theoretical models and numerics of COBRA-TF [7], and Conner et al. presented the Westinghouse CFD methodology to model single-phase, steady-state conditions in PWR fuel assemblies as well as benchmark testing in [8]. In the meantime, direct numerical simulation (DNS) approach has started to attract the community's attention as a promising tool in studying turbulence phenomena in nuclear reactors due to the rapid development of high performance computing. In DNS of turbulence, the equations of fluid motion (the Navier-Stokes equations) are solved, without turbulence closure assumptions (unlike classic CFD approach, or even more empirical subchannel analysis), with sufficient temporal and spatial resolution to represent all the scales of turbulence down to Kolmogorov scales [9, 10]. Ninokata and Baglietto have applied DNS to a fully-developed single phase turbulent flow analysis for triangular pin bundles [11, 12], but the Reynolds numbers resolved in their DNS are relatively low (up to Re_h of 24,300).

Besides the single-phase analysis, the study of two-phase turbulence phenomena inside fuel bundles is also of great importance to predict and analyze boiling flows which occur during normal operation and accident conditions in the reactor core. One of the major technological issues in the field of nuclear power is the departure from nucleate boiling (DNB) condition in the fuel assembly of a nuclear reactor core [13]. The development of new closure laws for computational multiphase fluid dynamics (CMFD) and subchannel analysis can utilize the detailed information provided by the high fidelity interface tracking simulations (ITS) of bubbly flows with DNS of liquid turbulence.

DNS of multiphase flows has been studied previously and provided unprecedented insight into complex flow phenomena. For example, Lu and Tryggvason (2008) studied a turbulent bubbly upflow in a vertical channel using front tracking method, and it was observed that the void fraction profile highly depends on the deformability of the simulated bubbles [14]. Bolotnov et al. also studied the turbulent bubbly flows in flat channels with DNS to investigate the bubble distribution and bubbles' influence on the turbulence field [15, 16]. Thomas et al. [17, 18] and Fang et al. [19] have implemented a proportional-integral-derivative

(PID) controller in ITS to evaluate the drag and lift forces a bubble experiencing in uniform shear flows, and the drag coefficients extracted achieve an excellent agreement with experimentally based correlations.

In the presented research, both single and two-phase turbulence are simulated within a PWR subchannel for Reynolds numbers (Re_h) of 29,079 and 80,774 (based on the hydraulic diameter and mean velocity). The turbulent flow of Reynolds number of 29,530 has been previously simulated in a flat channel [16] and will be compared with the case with Re_h of 29,079 to investigate the influence of PWR geometry on the turbulent flow structures. Since the mesh size for DNS grows exponentially as Re_h increases [10], the Reynolds number of 80,774 is chosen as the effort approaching to the simulations with realistic PWR conditions by considering the state-of-the-art computing resources (e.g. currently #5 supercomputer in the world, IBM BG/Q "Mira" at Argonne National Laboratory). Some preliminary results from the low Reynolds number case (29,079) have been presented in [20] from the limited statistical data available at that time, and since then much larger dataset has been collected to help us better understand the bubbly turbulence phenomena in the PWR subchannel. By processing the instantaneous data provided by DNS, statistical results obtained include the mean gas and liquid velocity profiles, void fraction distribution and turbulent kinetic energy profiles. The most novel aspect of current work is that DNS coupled with interface tracking method has been applied to the analysis of turbulent bubbly flows inside the PWR subchannel, which will help develop more accurate closure laws and ensure a higher quality prediction of single and two-phase turbulent flows for nuclear reactor designs.

2. NUMERICAL METHOD

2.1 Flow solver

The flow solver being used in the present work is PHASTA, which is a parallel, hierarchic, higher-order accurate, adaptive, stabilized (finite element) transient analysis flow solver for both incompressible and compressible flows. This approach has been shown to be an effective tool for bridging a broad range of length scales in turbulent (Reynolds averaged Navier-Stokes (RANS), large-eddy simulation (LES), detached eddy simulation (DES), DNS) flows [21, 22]. PHASTA was the first unstructured grid LES code [23] and has been applied to turbulent flows ranging from validation benchmarks (channel flow, decay of isotropic turbulence) to complex flows (airfoils at maximum lift, flow over a cavity, near lip jet engine flows and fin-tube heat exchangers). The PHASTA code uses advanced anisotropic adaptive algorithms [24] and the most advanced LES/DES models [25, 26]. This capability has been extended to two-phase flows where we use the level set method to track the boundary between two immiscible fluids [15, 27]. The highly scalable performance of PHASTA on massively parallel computers has already been demonstrated [28] (the code has shown good scaling up to 768×1024 processors on the IBM Blue Gene/Q Mira system, (ANL, #5 in top500 as of November 2014)).

In the simulations the fluid is assumed to be isothermal and incompressible. The strong form of the incompressible Navier-Stokes (INS) is given by

Continuity:
$$\frac{\partial u_i}{\partial x_i} = 0 \tag{1}$$

Momentum:
$$\rho \frac{\partial u_i}{\partial t} + \rho u_j \frac{\partial u_i}{\partial x_j} = -\frac{\partial p}{\partial x_i} + \frac{\partial \tau_{ij}}{\partial x_j} + f_i \tag{2}$$

where u_i is the velocity in the x_i-direction, ρ denotes the density of the fluid, p the static pressure and τ_{ij} the viscous stress tensor. For the incompressible flow of a Newtonian fluid, the viscous stress tensor is related to the fluid viscosity and the strain rate tensor as:

$$\tau_{ij} = 2\mu S_{ij} = \mu(\frac{\partial u_i}{\partial x_j} + \frac{\partial u_j}{\partial x_i}) \quad (3)$$

In order to extend PHASTA's capability from single-phase to two-phase flows, the level set interface tracking method [29, 30, 31] was implemented. The interface is modeled as the zero-level set of a smooth function, φ, where φ is called the first scalar and is represented as the signed distance from the zero-level set. At $\varphi = 0$, the level set defines the interface. The scalar, φ, is advected with the fluid according to the advection Eq. (4) described in [29]. The liquid phase is indicated by a positive level set, $\varphi > 0$, while the gas phase by a negative level set, $\varphi < 0$.

$$\frac{\partial \varphi}{\partial t} + u_j \frac{\partial \varphi}{\partial x_j} = 0 \quad (4)$$

The Continuum Surface Tension (CST) model [32] is used in PHASTA to compute the surface tension force as a local interfacial force density, which is included in the body force term on the right hand side of the INS equations.

Evaluating the jump in physical properties across the interface using a step change lis challenging numerically; therefore, the properties near the interface are defined using a smoothed Heaviside kernel function, H_ε [31]. While the solution may be relatively good in the close vicinity of the interface, the distance field, φ, may not be correct elsewhere in the domain where the varying fluid velocities throughout the flow field distort the level set contours (such as in a fully resolved turbulent flow). To maintain a true distance field, the level set is corrected at every time iteration with a re-distancing operation [33]. A detailed description of the equations and re-distancing process used can be found in [15].

2.2 DNS mesh design

The following requirements must be met to ensure an accurate representation of all relevant scales in PHASTA simulations: (i) The computational domain must be sufficiently large to contain the largest turbulent eddies, and (ii) the grid spacing must be sufficiently fine in order to capture the smaller scales of interest (e.g. Kolmogorov turbulent length scale). The first requirement is met if two-point correlations in the streamwise and spanwise directions vanish within one-half of the computational domain [10]. Meanwhile, the number of mesh points in physical domain must be chosen to resolve the finest scale of appreciable excitation, namely layers of the Kolmogorov dissipation scale thickness [34]. The first plane of grid points off the walls was at a normalized distance of 1.0 (y^+) discussed in [35]. More discussions regarding the DNS resolution requirements for turbulent flows can also be found in [36, 37].

3. PROBLEM DESCRIPTION

To create a single PWR subchannel domain, the model is first built in CAD software (e.g. SolidWorks), which can be then utilized by meshing tools (provided by Simmetrix, Inc. in our case) to generate the corresponding unstructured mesh. Certain number of boundary layers is specified near the fuel rod surface to capture the detailed information regarding the turbulence in the region very close to walls, governed by well-known law of the wall [35]. The mesh size is 53.8 million elements for the case of Re_h of 29,079. Recent progress in advanced parallel meshing tool allows us to generate much larger meshes to fully resolve the turbulence of higher Reynolds numbers, and for the case with Re_h of 80,774 the mesh created includes 1.11 billion elements partitioned into 131,072 parts. Both the domain overview and a zoom-in view for the boundary layers are shown in Figure 1. The length of the subchannel corresponds to about 3 hydraulic diameters (40.5 mm), which is calculated based on the cross section area and perimeter shown in Eq. (5). The direction of gravity is opposite to the mean flow direction, which represents an upward flow in a vertical

subchannel. The cases of two Reynolds numbers are labeled with RE01 (for Re_h of 29,079) and RE02 (for Re_h of 80,774). More detailed discretization parameters are listed in Table I, including domain sizes and resolutions.

$$D_h = \frac{4A}{p} \tag{5}$$

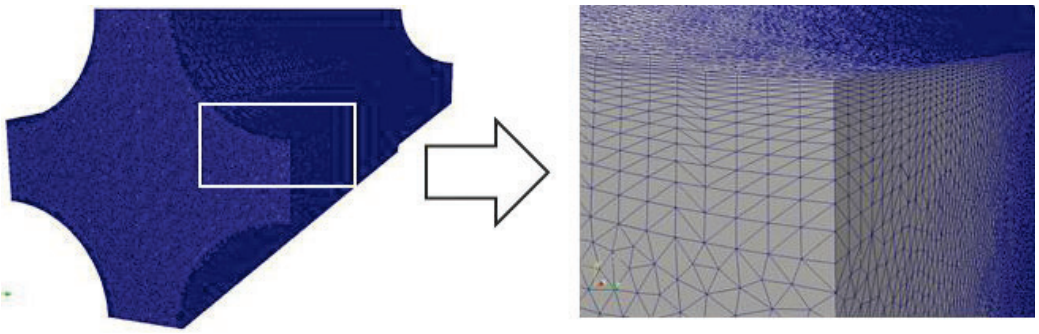

Figure 1. Typical unstructured mesh with boundary layers

Table I. Discretization parameters

Case	RE01	RE02
Domain sizes (mm)	40.5x12.6x12.6	
Rod radius (mm)	4.57	
Reynolds number resolved (Re_h)	29,079	80,774
Resolved bubble diameter (mm)	1.6210	0.6509
Bulk resolution (mm)	8.11×10^{-2}	3.25×10^{-2}
Bubble surface CFL number	0.21	0.39
Maximum CFL number in the domain	7.5	8.0
Thickness of first B. L. (y^+=1) (mm)	8.11×10^{-3}	3.25×10^{-3}
Number of boundary Layers	13	13
Number of points	9,249,506	186,825,949
Number of elements	53,837,248	1,111,168,768
Number of computing cores used	8,192	131,072
Element per core	6,572	8,478

Periodic boundary conditions are utilized to represent a much longer domain than computationally feasible in DNS approach and to be able to achieve statistically steady state flow conditions. The domain is periodic

at inflow and outflow planes as well as the transverse faces, and no-slip wall conditions are applied to the fuel rod surface (Figure 2).

The DNS turbulent results for both single and two-phase flows are produced efficiently using a two-step approach. The single-phase turbulent velocity profile is first generated by placing a sphere blockage region at the domain center to create fluctuations. After large turbulence structures are observed the spherical barrier is removed and the flow can sustain turbulence. The statistical data is recorded at this point; the convergent behavior is observed as steady state is achieved as shown in Figure 7. When we ensured that the single phase turbulence has achieved statistically steady state flow conditions by comparing averaged velocity profiles over different time windows, the second step was performed to initialize the bubbles (representing a 1% bubble volume fraction), and bubbles' motion and deformation are resolved using level-set interface tracking method. The detailed bubble initialization process has been descripted previously in [20].

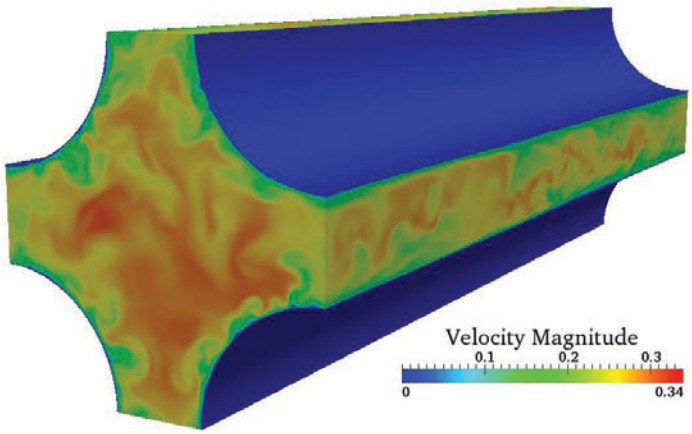

Figure 2. Wall condition in the subchannel simulations

Considering both computational cost and quality of the results (based on previous resolution and validation studies) the resolution for bubbles is set to be 20 elements across diameter, which results in 17 bubbles for the 53.8 M mesh and 262 bubbles for the 1.11 B mesh at the 1% volumetric fraction. The scaling studies have shown that the most efficient approach is to use 4 message-passing-interface (MPI) partitions per physical core on Mira supercomputer and this results in computational cost of 26.8K CPU-hours for RE01 case and 730K CPU-hours for RE02 case to achieve one domain flow-through (about 3.14 L/D length). Higher resolution will result in the rapid increase of computational cost while lower resolution is not capable to capture enough details regarding bubbles' behaviors to reach meaningful conclusions. As shown in Figure 5, a set of virtual probes are designed and placed near outflow plane to record instantaneous velocity fluctuations and bubble distribution across the domain. The bubble distribution and turbulence for 17 bubbles and 262 bubbles are shown in Figure 3 and Figure 4 (the direction of mean flow is from left to right as pointed by the red arrow at bottom-left of figures). Interface tracking simulations are run with the bubbles to allow the flow to fully develop and the bubbles to achieve their terminal velocities.

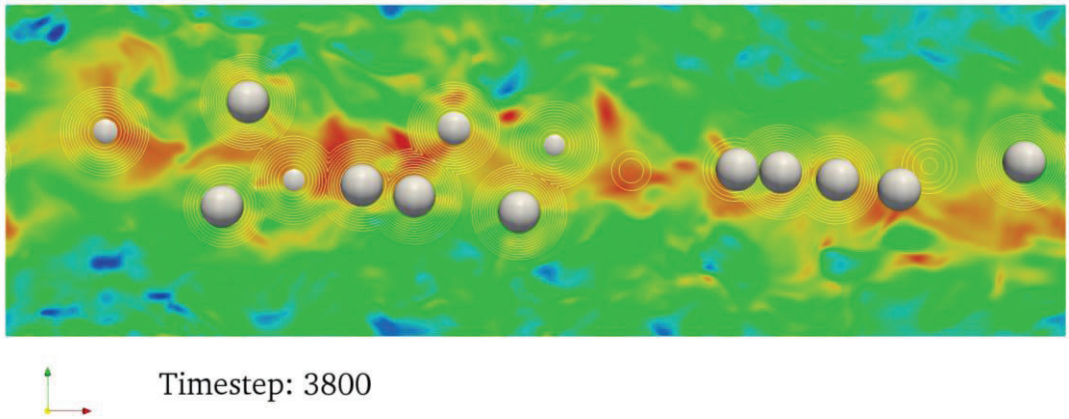

Figure 3. Distribution of 17 bubbles in the turbulent flow (half of the domain can be seen).

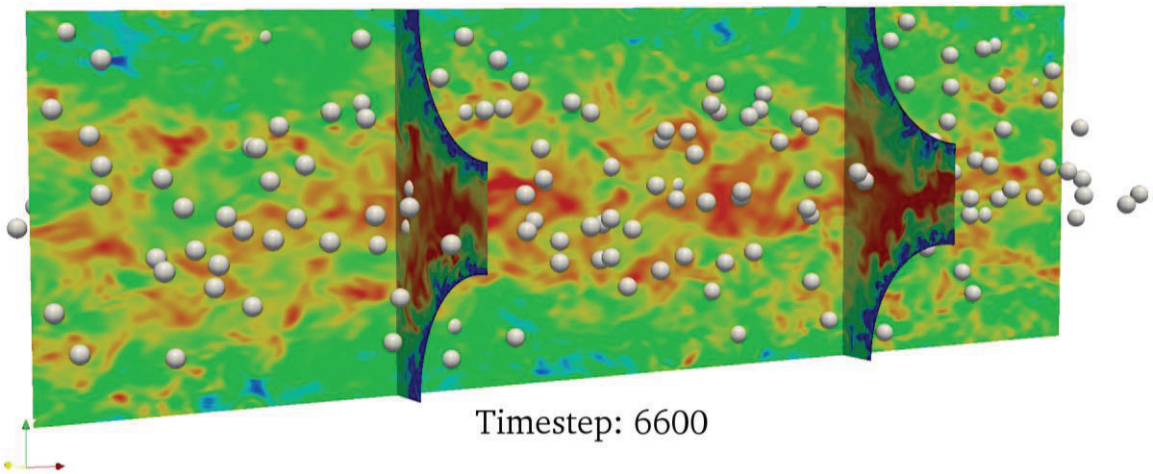

Figure 4. Distribution of 262 bubbles in the turbulent flow

The key computational parameters and fluid properties are listed in Table II. The viscosities and densities of liquid/gas are determined by using the saturated properties of water and vapor at 300 ℃. The estimation of realistic PWR conditions can be found in [38]. The data collected from the simulations is processed to obtain, for instance, the mean velocity (U_i) and turbulent kinetic energy (k) that are calculated based on Eqs. (6) and (7). The probes used to extract the flow statistics are shown in Figure 5 and their location has been improved based on the previous design used in [20]. New probe design is more reasonable, in particular with a much larger distribution density in the boundary layer region in order to capture the flow behavior near the walls.

$$U_i(t) = \frac{1}{N_w}\sum_{j=1}^{N_w} u_i(t + t_j) \tag{6}$$

$$k(t) = \frac{1}{N_w}\sum_{j=1}^{N_w}\sum_{i=1}^{3}\frac{1}{2}u_i'(t + t_j)^2 \tag{7}$$

where, $u_i'(t+t_j) = u_i(t+t_j) - U_i(t)$ is the fluctuation of velocity component-i computed at the time instant $t+t_j$; N_w is the number of velocity samples in each window, t is the current time, $t_j = (j - N_w/2)\Delta t$ is the local window time, and Δt is the time step. Two-phase flows additional parameters, such as void fraction and phasic velocities are also determined using this basic statistical analysis method.

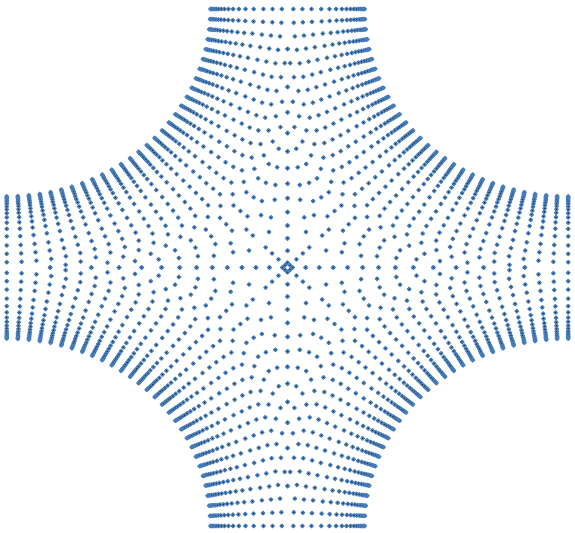

Figure 5. Improved probe design with more reasonable distribution

Table II. Fluid properties used in the simulations

Case	RE01	RE02	Realistic PWR condition
Liquid/Gas Viscosities (Pa·s)	8.585×10^{-5}; 1.965×10^{-5}		
Liquid/Gas Densities (kg/m^3)	712.22; 46.17		
Mean velocity (m/s)	0.27	0.75	4.62
Reynolds number (Re_h)	29,079	80,774	452,500

4. RESULTS AND DISCUSSION

Both single- and two-phase subchannel simulations were performed on IBM BG/Q "Mira" at the Leadership Computing Facility (ALCF) located at the Argonne National Laboratory. The simulation results were visualized using the open-source software, ParaView. The scaling performance of the parallel DNS flow solver, PHASTA, was investigated for subchannel cases before the production runs. A set of standard parameters were adopted in all tests and the only difference is the number of mesh partitions. The results obtained confirmed our previous experience [28] that PHASTA scales very well for massively parallel computations of interest. The simulation efficiency is measured in core-hours consumed to conduct one full time step for each 1 billion element. Each node on "Mira" has 16 cores while each core is able to perform up to 4 MPI processes, and we observed that 4-mpi per core runs lead to the most efficient simulations, which means 4-mpi per core runs consume the least core-hours with the same mesh partitions. The computational efficiency in cases with smaller partition counts is not as good because the number of elements each core has to compute exceeds the limit that a core can efficiently handle due to memory cache

limits. As expected, for partitions numbers higher than 65,536, the efficiency is slightly reduced due to increasing burden from inter-processor communications.

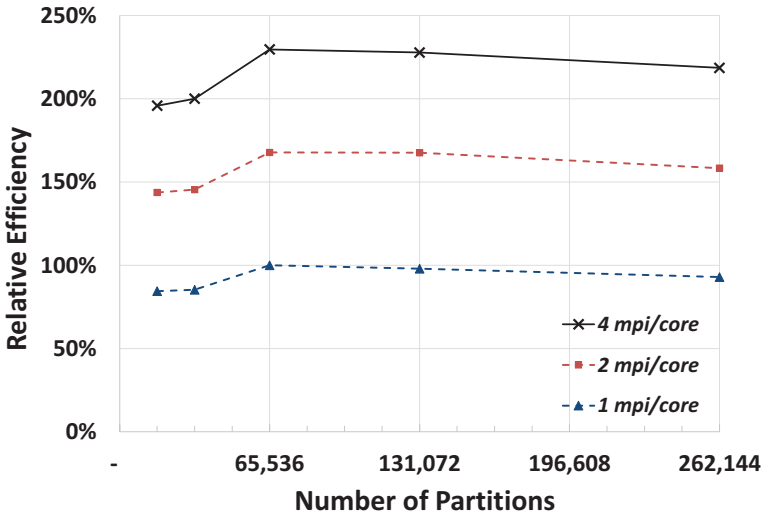

Figure 6. Scaling results of PHASTA on Mira BG/Q with a 1.11 B element mesh (subchannel geometry) normalized using 1 mpi/core run at 64K parts.

Law of the wall profiles shown in Figure 7 with dashed line results in the coefficients of $B = 5.8$ and $\kappa = 0.39$ observed in the single-phase RE01 simulations and $B = 5.5$ and $\kappa = 0.37$ for single-phase RE02 cases:

$$U^+ = \frac{1}{\kappa}\log y^+ + B \tag{8}$$

These are expected constants for the turbulent law of the wall. We have previously observed the values of $B = 5.5$ and $\kappa = 0.4$ for a rectangular channel which were validated against available data and analytical correlations [39]. Fluctuations in law of the wall measured above are observed for large y^+ (200~400 for RE01 and 900~1300 range for RE02) which does not follow classic flat channel behavior. This behavior is related to the geometry of the subchannel: turbulent flow behavior at the center of subchannel is affected by all four rod walls and thus different from the law of the wall in the boundary layer/rectangular geometry.

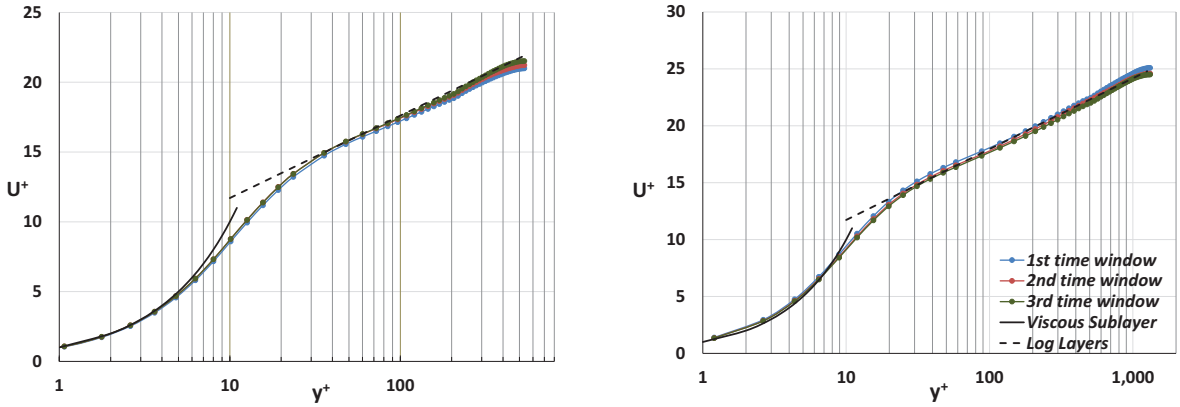

Figure 7. Law of the wall profile for single phase simulations (left: RE01, right: RE02)

The turbulent kinetic energy profile and dimensionless velocity profile are also captured by analyzing the DNS data statistically (Figure 8). Interestingly, there is a flattened region on turbulent kinetic energy's decaying tail for both RE01 and RE02 cases as shown in Figure 8, and distance to the subchannel rod for this inflection is 1.85 mm, which is very close to the half minimum distance between fuel rods (1.71 mm in our cases). As we can see in Figure 5, the probes at the same distance to fuel rod wall can experience different turbulent flow near the center of the subchannel compared to the boundaries. The statistical analysis tools we use are averaging the data from the probes located at a constant distance from the walls to produce each of the point in Figure 8. At the larger distance from the wall, beyond the minimum half-distance between the fuel rods, the averaging occurs over smaller azimuthal region around each fuel rod. This causes the described behavior at the y^+ = 250-300 range shown in Figure 7 for cases RE01 and y^+ = 550-600 in case RE02.

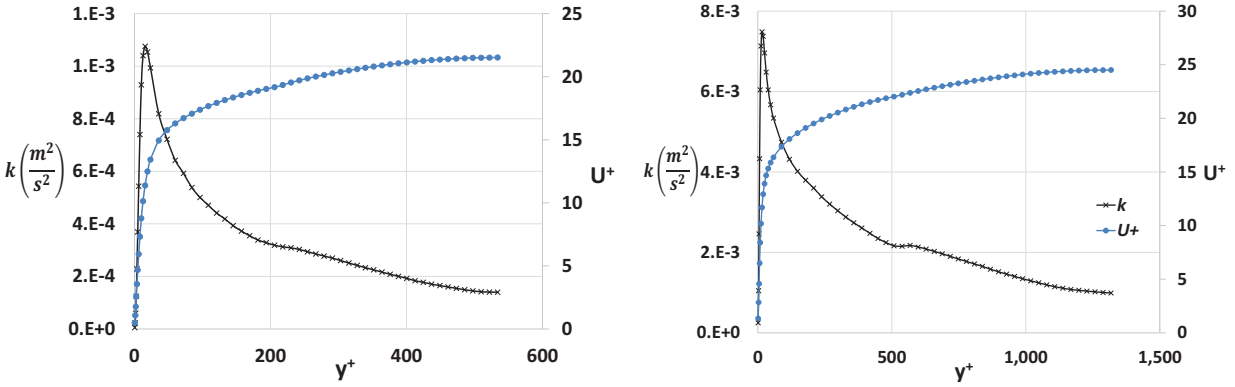

Figure 8. Turbulent kinetic energy and dimensionless velocity for single-phase simulations (left: RE01, right: RE02)

Once statistically convergent flow is obtained for the single phase subchannel the bubbles are introduced in the domain through the level set method. Generally, two-phase simulations impose stricter requirements on the flow solver, such as smaller CFL number around the bubbles to properly resolve bubble deformation and advection and larger number of iterations at each time step. In addition, more simulation time is needed to accurately compute the bubble void fraction distribution for low void fraction flows due to much smaller data available for the gas phase compared to the liquid phase. The initial condition for the bubbles was specified as the distance field scalar. Seventeen bubbles were initialized in case RE01 and 262 bubbles in case RE02 to represent 1% gas volume fraction two-phase flow (as shown in Figure 3 and Figure 4). We intend to obtain statistically significant data in both cases to analyze the void fraction distribution, as well as gas and liquid mean velocity profiles. Coalescence occurs in the simulations of two-phase RE01, which hinders us from studying the influence of bubbles with a certain size on turbulence in the subchannel. Since the coalescence effects cannot be neglected within the 17-bubble two phase simulations, the coalescence control has been recently developed [40] and is applied to the 17-bubble RE01 simulations. Considering the potential computational cost of coalescence control, the control is not activated in 262-bubble RE02 simulations if the coalescence effect can be mitigated in the case of a large number of bubbles.

As illustrated in Figure 9, Figure 10 and Figure 11, we have statistically processed the recorded data from the two-phase RE01 and RE02 simulations. The turbulent bubbly flows have achieved 2 flow-throughs in RE01 case and 1.67 flow-throughs in RE02 cases. Law of the wall analysis shown in Figure 9 with dashed line results in the coefficients of B = 8.3 and κ = 0.55 observed in the two-phase RE01 simulations and B = 4.8 and κ = 0.35 for two-phase RE02 cases. Compared with the results from RE02 simulations, RE01

two-phase cases exhibited more fluctuations and the law of the wall profile in has been flattened. One should keep in mind that RE02 two-phase cases can resolve many more smaller bubbles, so larger number of bubble instances will be detected by probes during one flow through. Thus, better statistics were obtained for 262 bubble simulations (RE02) vs. 17 bubble simulation (RE01).

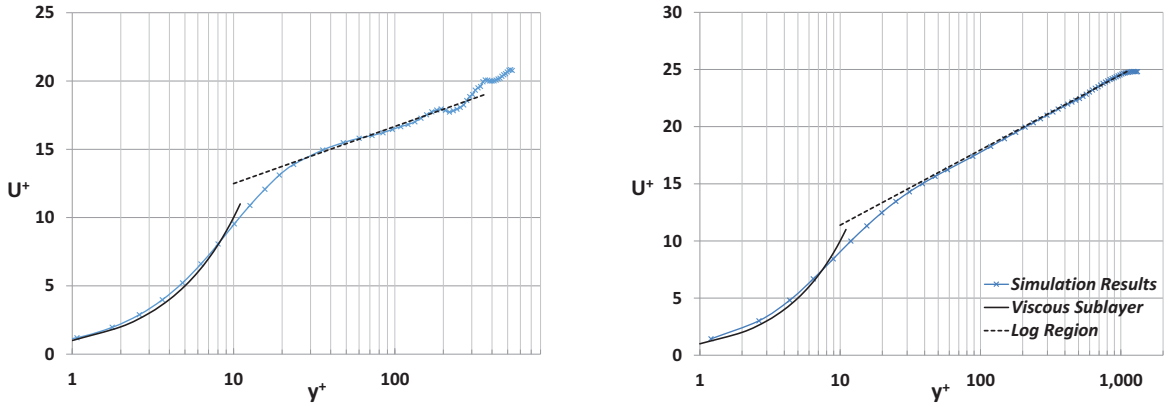

Figure 9. Law of the wall profile for two-phase simulations (left: RE01, right: RE02). The viscous sublayer curve shown is described by $u^+ = y^+$ and the log law is described by Eq. (8).

In contrast to the TKE profile in the single-phase RE01 case, the TKE profile of two-phase RE01 case shows a prominent peak which corresponds to the contribution of the bubbles as shown in Figure 10 (left). However, the peak on the TKE decaying tail from RE02 is not as significant as RE01, which could be related to the smaller bubble size. Also the magnitude of TKE in RE02 is notably higher than that in RE01. The distributions of gas and liquid velocity as well as the void fraction from the two-phase RE01 and RE02 simulations are shown in Figure 11. In the region where the void fraction is higher than 0, the corresponding gas velocity is observed to be larger than liquid velocity because the bubbles are accelerated by the buoyancy force in the subchannel. In the RE02 262 bubble case, the void fraction peak moves closer to the subchannel walls as expected because smaller bubbles will migrate in transverse directions due to the effect of the lift force. When two-phase flows achieve statistically steady state conditions, the drag coefficient can be estimated based on the bubbly buoyancy force and bubble terminal velocity. Assuming that the steady state conditions are reached and by averaging the bubble relative velocities we can utilize the force balance between the drag and buoyancy forces on the bubble and estimate the drag coefficient of 0.498 in RE01 two-phase case and 0.658 in RE02 two-phase case.

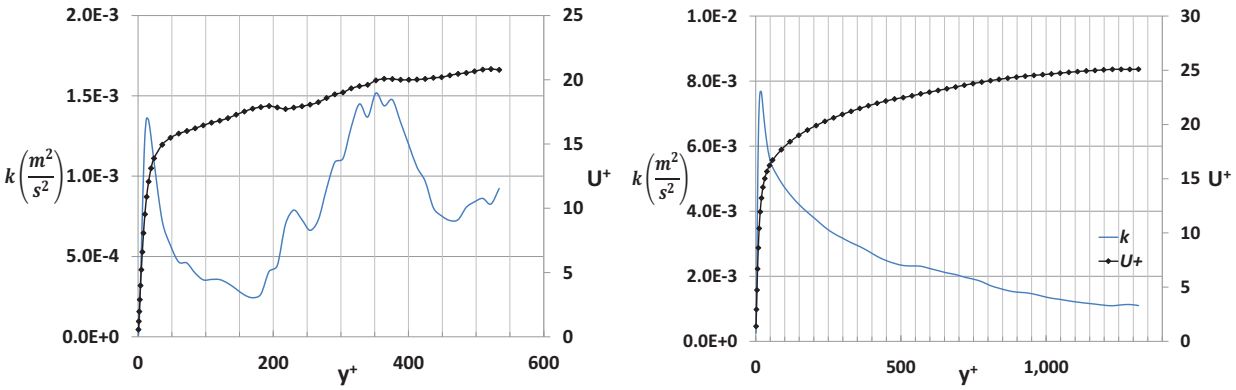

Figure 10. Turbulent kinetic energy and dimensionless velocity for two phase cases (left: RE01, right: RE02)

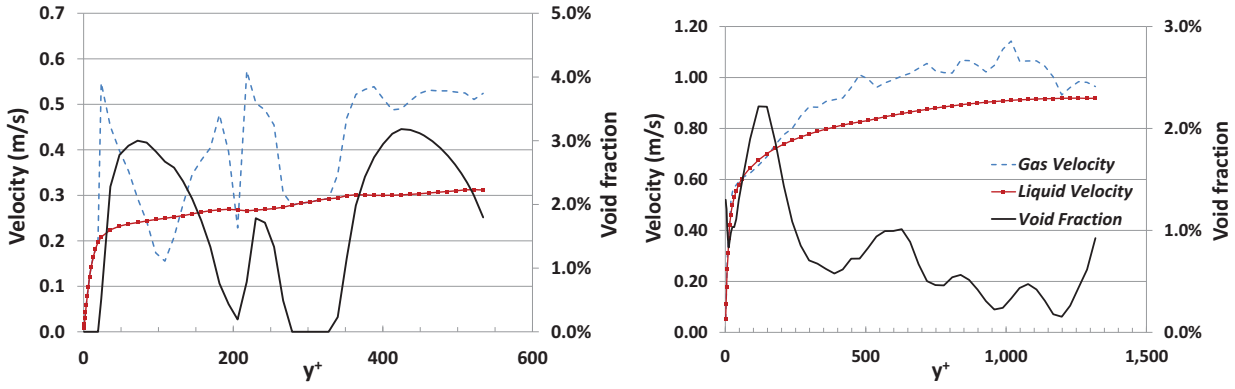

Figure 11. Void fraction and gas-liquid velocity profile from two-phase simulations (left: RE01, right: RE02)

5. CONCLUSIONS

Latest results on DNS/ITM simulations in subchannel flow geometry for single and two-phase turbulent flows are presented. While the computational cost remains a big challenge for larger domains and high Reynolds number simulations, the current capabilities clearly demonstrate that DNS/ITM approach can be a valuable and promising tool to guide the development of CMFD models as well as subchannel closure laws for nuclear reactor applications. We have shown the single-phase law of the wall constants from the subchannel turbulence are similar to the ones observed in the parallel plates geometry, and the constants may change in the presence of bubbles. The bubble aggregation near the fuel rods is observed in the 262 bubble RE02 case as expected due to the lift force effect. Future work will include collecting more statistical data, as well as the advanced analysis of individual bubble behavior to provide additional insights for subchannel turbulent bubbly flows. These studies will help to determine if the existing turbulence models and interfacial forces closure laws developed for pipe and channel flows can be directly applied to multiphase CFD in reactor subchannels.

ACKNOWLEDGMENTS

The authors would like to acknowledge the support from Consortium for Advanced Simulation of Light Water Reactors (http://www.casl.gov), an Energy Innovation Hub (http://www.energy.gov/hubs) for Modeling and Simulation of Nuclear Reactors under U.S. Department of Energy [grant number DE-AC05-00OR22725]. An award of computer time was provided by the ASCR Leadership Computing Challenge (ALCC) program. This research used resources of the Argonne Leadership Computing Facility, which is a DOE Office of Science User Facility supported under Contract DE-AC02-06CH11357. The solution presented herein made use of the Acusim linear algebra solution library provided by Altair Engineering Inc. and meshing and geometric modeling libraries by Simmetrix Inc.

REFERENCES

1. Trupp, A. C., & Azad, R. "The structure of turbulent flow in triangular array rod bundles," *Nuclear Engineering and Design,* **32**(1), pp. 47-84 (1975).
2. Carajilescov, P., & Todreas, N. "Experimental and analytical study of axial turbulent flows in an interior subchannel of a bare rod bundle," *Journal of Heat Transfer,* **98**(2), pp. 262-268 (1976).
3. Rehme, K. "Experimental observations of turbulent flow through subchannels of rod bundles," *Experimental Thermal and Fluid Science,* **2**(3), pp. 341-349 (1989).

4. Wu, X., & Trupp, A. "Experimental study on the unusual turbulence intensity distributions in rod-to-wall gap regions," *Experimental Thermal and Fluid Science,* **6**(4), pp. 360-370 (1993).
5. Dominguez-Ontiveros, E. E., & Hassan, Y. A. "Non-intrusive experimental investigation of flow behavior inside a 5× 5 rod bundle with spacer grids using PIV and MIR," *Nuclear Engineering and Design,* **239**(5), pp. 888-898 (2009).
6. Thurgood, M. *COBRA/TRAC, a thermal-hydraulics code for transient analysis of nuclear reactor vessels and primary coolant systems.* The Commission. (1983).
7. Avramova, M. "Development of an innovative spacer grid model utilizing computational fluid dynamics within a subchannel analysis tool," (Ph.D. Dissertation, The Pennsylvania State University). (2007).
8. Conner, M. E., Baglietto, E., & Elmahdi, A. M. "CFD methodology and validation for single-phase flow in PWR fuel assemblies," *Nuclear Engineering and Design,* **240**(9), pp. 2088-2095 (2010).
9. Lee, M., Malaya, N., & Moser, R. D. "Petascale direct numerical simulation of turbulent channel flow on up to 786k cores," Paper presented at the *Proceedings of SC13: International Conference for High Performance Computing, Networking, Storage and Analysis,* pp. 61 (2013).
10. Trofimova, A. V., Tejada-Martínez, A. E., Jansen, K. E., & Lahey Jr, R. T. "Direct numerical simulation of turbulent channel flows using a stabilized finite element method," *Computers & Fluids,* **38**(4), pp. 924-938 (2009).
11. Ninokata, H., Atake, N., Baglietto, E., Misawa, T., & Kano, T. "Direct numerical simulation of turbulent flows in a subchannel of tight lattice fuel pin bundles of nuclear reactors," *Annual Report of the Earth Simulator Center April,* **2005** (2004).
12. Baglietto, E., Ninokata, H., & Misawa, T. "CFD and DNS methodologies development for fuel bundle simulations," *Nuclear Engineering and Design,* **236**(14), pp. 1503-1510 (2006).
13. Anglart, H., & Nylund, O. "CFD application to prediction of void distribution in two-phase bubbly flows in rod bundles," *Nuclear Engineering and Design,* **163**(1), pp. 81-98 (1996).
14. Lu, J., & Tryggvason, G. "Effect of bubble deformability in turbulent bubbly upflow in a vertical channel," *Physics of Fluids (1994-Present),* **20**(4), pp. 040701 (2008).
15. Bolotnov, I. A., Jansen, K. E., Drew, D. A., Oberai, A. A., & Lahey, J. T.,R. "Detached direct numerical simulation of turbulent two-phase bubbly channel flow," *International Journal of Multiphase Flow,* **37**, pp. 647-659 (2011).
16. Bolotnov, I. A. "Influence of bubbles on the turbulence anisotropy," *Journal of Fluids Engineering,* **135**(5), pp. 051301 (2013).
17. Thomas, A. M., Fang, J., & Bolotnov, I. A. "Estimation of shear-induced lift force in laminar and turbulent flows," *International Topical Meeting on Advances in Thermal Hydraulics - 2014 (ATH '14),* Reno, NV. (2014).
18. Thomas, A. M., & Bolotnov, I. A. "Evaluating shear induced lift force using interface tracking approach," *Transactions of the 2012 ANS Winter Meeting,* San Diego, CA., Vol. 107, pp. 1277-1278 (2012).
19. Fang, J., Thomas, A. M., & Bolotnov, I. A. "Development of advanced analysis tools for interface tracking simulations," *Transactions of the 2013 ANS Winter Meeting,* Washington D.C., Vol. 109, pp. 1613-1615 (2013).
20. Fang, J., Mishra, A. V., & Bolotnov, I. A. "Interface tracking simulation of two-phase bubbly flow in A PWR subchannel," *International Embedded Topical Meeting on Advances in Thermal Hydraulics - 2014 (ATH '14),* Reno, NV. (2014).
21. Jansen, K. E. "A stabilized finite element method for computing turbulence," *Computer Methods in Applied Mechanics and Engineering,* **174**(3), pp. 299-317 (1999).

22. Whiting, C. H., & Jansen, K. E. "A stabilized finite element method for the incompressible navier-stokes equations using a hierarchical basis," *International Journal for Numerical Methods in Fluids,* **35**(1), pp. 93-116 (2001).
23. Jansen, K. E. "Unstructured grid large eddy simulations of wall bounded flows," *Annual Research Briefs, Center for Turbulence Research, NASA Ames/Stanford University,* pp. 151 (1993).
24. Sahni, O., Müller, J., Jansen, K., Shephard, M., & Taylor, C. "Efficient anisotropic adaptive discretization of the cardiovascular system," *Computer Methods in Applied Mechanics and Engineering,* **195**(41), pp. 5634-5655 (2006).
25. Tejada-Martínez, A. E., & Jansen, K. E. "A parameter-free dynamic subgrid-scale model for large-eddy simulation," *Computer Methods in Applied Mechanics and Engineering,* **195**(23), pp. 2919-2938 (2006).
26. Spalart, P. R., Deck, S., Shur, M. L., Squires, K. D., Strelets, M. K., & Travin, A. "A new version of detached-eddy simulation, resistant to ambiguous grid densities," *Theoretical and Computational Fluid Dynamics,* **20**(3), pp. 181-195 (2006).
27. Nagrath, S., Jansen, K., Lahey Jr, R. T., & Akhatov, I. "Hydrodynamic simulation of air bubble implosion using a level set approach," *Journal of Computational Physics,* **215**(1), pp. 98-132 (2006).
28. Rasquin, M., Smith, C., Chitale, K., Seol, E. S., Matthews, B. A., Martin, J. L., . . . Jansen, K. E. "Scalable implicit flow solver for realistic wing simulations with flow control," *Computing in Science & Engineering,* **16**(6), pp. 13-21 (2014).
29. Sussman, M., Fatemi, E., Smereka, P., & Osher, S. "An improved level set method for incompressible two-phase flows," *Computers & Fluids,* **27**(5), pp. 663-680 (1998).
30. Sethian, A. J. *Level set methods and fast marching methods.* Cambridge University Press. (1999).
31. Sussman, M., Almgren, A. S., Bell, J. B., Colella, P., Howell, L. H., & Welcome, M. L. "An adaptive level set approach for incompressible two-phase flows," *Journal of Computational Physics,* **148**(1), pp. 81-124 (1999).
32. Brackbill, J. U., Kothe, D. B., & Zemach, C. "A continuum method for modeling surface tension," *Journal of Computational Physics,* **100**(2), pp. 335-354 (1992).
33. Fatemi, E., & Sussman, M. "An efficient interface preserving level-set re-distancing algorithm and its application to interfacial incompressible fluid flow," *SIAM J Sci Statist Comput,* **158**(1), pp. 36 (1995).
34. Orszag, S. A. "Analytical theories of turbulence," *Journal of Fluid Mechanics,* **41**(02), pp. 363-386 (1970).
35. Pope, S. B. *Turbulent flows.* Cambridge university press. (2000).
36. Kim, J., Moin, P., & Moser, R. "Turbulence statistics in fully developed channel flow at low reynolds number," *Journal of Fluid Mechanics,* **177**, pp. 133-166 (1987).
37. Moser, R. D., Kim, J., & Mansour, N. N. "Direct numerical simulation of turbulent channel flow up to re= 590," *Phys. Fluids,* **11**(4), pp. 943-945 (1999).
38. Thomas, A. M. "Estimation of the shear-induced lift force on a single bubble in laminar and turbulent shear flows using interface tracking approach," (M.S. Thesis, North Carolina State University). (2014).
39. Mishra, A. V., & Bolotnov, I. A. "DNS of turbulent flow with hemispherical wall roughness," *Journal of Turbulence,* **16**(3), pp. 225-249 (2015).
40. Talley, M. L. "Bubble coalescence control development for level set interface tracking method," (M.S. Thesis, North Carolina State University). (2014).